Femtosecond Photolysis of HOCl(aq): Dissipation of Fragment Kinetic Energy

D. Madsen, C. L. Thomsen, J. Aa. Poulsen, S. J. Knak Jensen, J. Thøgersen, and S. R. Keiding*

Department of Chemistry, University of Aarhus, Langelandsgade 140, DK-8000 Aarhus C, Denmark

E. B. Krissinel

European Bioinformatics Institute Genome Campus, Hinxton Cambridge CB10 1SD, U.K.

Received: September 11, 2002; In Final Form: November 15, 2002

In this work, we present an experimental study of the energy dependence of the photolysis of aqueous HOCl and the subsequent recombination of the OH and Cl photofragments. Using femtosecond transient absorption spectroscopy, we follow the time-dependent concentration of the fragments. The excess energy in the photolysis is given to the fragments as kinetic energy, and tuning the wavelength enables a study of the energy-dependent thermalization and geminate recombination of the fragments in the liquid environment. The recombination yield and rate are governed by the initial fragment separation, and we deduce an approximately linear dependence of the fragment separation versus the kinetic energy with a slope of 0.13 nm/eV. Performing a simple MD simulation of the system gives qualitative agreement with the observations, although the calculated slope is only 0.04 nm/eV.

I. Introduction

In this work, we study the energy dependence of the geminate recombination of OH and Cl following femtosecond photolysis of aqueous HOCl. We have previously shown that aqueous HOCl offers a well-suited and simple system for studying the fundamental solute−solvent interactions taking place during bond breaking and the subsequent recombination.[1] When photolyzed at wavelengths below 340 nm, the isolated HOCl molecule dissociates to Cl and OH. The majority of the excess energy is converted into the kinetic energy of the Cl and OH fragments with little vibrational excitation of the OH fragment.[1−4] When excited at 266 nm, the kinetic energy that is released is on the order of 2.5 eV (∼240 kJ/mol). This energy is sufficient for the fragments to escape the aqueous solvent cage, leading to a negligible quantum yield for geminate recombination within the first solvation shell. The escaping fragments thermalize through interaction with the solvent and may subsequently recombine by diffusive geminate recombination occurring on a 10−100 ps time scale. The quantum yield for diffusive geminate recombination depends on the initial separation of the fragments, which for HOCl(aq) becomes an experimentally accessible parameter through the tuning of the photolysis wavelength. This makes HOCl particularly well suited for experimental and theoretical studies of solvent−solute interaction, in particular the "stopping power" of the solvent (i.e., the ability to thermalize the translational energy of the recoiling reaction products).

Recently, detailed experimental and theoretical studies of caging, recombination, and cage escape have intensified, spurred by advances in ultrashort pulse laser technology. Experimentally, model systems based on either halogens trapped in rare gas matrices,[5] molecular beams of I_2^- in CO_2 or Ar clusters,[6] or I_2 in rare gases[7] at high pressure have provided valuable insight into the ultrafast dynamics of caging phenomena and recombination. Femtosecond studies of the kinetic energy tuning of the photofragments, as reported here, has to our knowledge been reported only once before, namely, in OClO.[8] In that work, the increase in cage escape along the O···ClO coordinate in OClO with decreasing photolysis wavelength was investigated. The cage escape grew approximately linearly with photon energy when the photolysis wavelength was tuned from 400 to 320 nm. However, the presence of a barrier in the upper electronic $\tilde{A}^2A_2$ state of OClO and the unknown distribution of energy among intra- and intermolecular degrees of freedom complicated the interpretation of the experimental data.

The theoretical work on caging and recombination can be divided into models using a continuum approach and discrete (microscopic) models. The continuum models[9,10] have their origin in the classic works of Smoluchowski[11] and Noyes[12] and are based on the diffusive motion of fragments in a continuous solvent, typically described by a friction coefficient. The continuum descriptions have successfully been applied to numerous nano- and picosecond experiments[13] on the caging and recombination of iodine. Very efficient and flexible numerical codes modeling such processes are generally available.[14] The microscopic models of photodissociation in solution are primarily based on molecular dynamics (MD) simulations, where fragment trajectories are calculated by classical propagation on the intermolecular potential describing the solvent−solute interactions. The most detailed microscopic model has been developed for systems of dihalogens in rare gas matrices. In these systems, a mixed quantum−classical description is formulated for the coupling between the electronic and nuclear coordinates of the dihalogen solutes *and* the electronic and nuclear degrees of freedom of the rare-gas solvent. In this description, it is possible to monitor simultaneously the trajectories of the caged fragments *and* the nonadiabatic transitions among the electronic states of the parent molecule.[5] These methods have not yet been applied to caging−recombination processes in real room-temperature liquids.

* Corresponding author. E-mail: keiding@chem.au.dk.

10.1021/jp026968u CCC: $25.00
Published on Web 04/10/2003

In this work, we present a detailed experimental and theoretical investigation of the photodissociation of HOCl and subsequent thermalization of the hot fragments by interaction with the solvent molecules. We follow these processes by monitoring the femtosecond transient dynamics of the chlorine photofragments as function of the photolysis wavelength, which in the present system directly dictates the kinetic energy of the photofragments. From the experimental data, we extract the initial fragment separation using a diffusion model. Because the separation derived from this analysis is very short, on the order 1 nm, we have, in addition to the classical continuum model, also modeled the experiment using molecular dynamics simulations.

The paper is organized as follows: Section II briefly describes the experimental procedures for synthesizing and characterizing HOCl and the photolytic products (Cl, OH) and the generation of the different pump wavelengths. Section III describes the experimental results obtained whereas section IV contains the data analysis and discussion.

II. Experimental Section

An aqueous solution of hypochlorous acid (HOCl) was synthesized by the method described by Cady.[15] The procedure, described in detail in ref 1, typically resulted in a HOCl(aq) concentration of ~1.5 M. The concentration and purity of the sample were determined by static UV−vis absorption using previously reported extinction coefficients for HOCl, ClOCl, and Cl_2 in aqueous solution. The HOCl solution was exchanged frequently during the series of measurements, and the flow was adjusted to ensure a fresh sample of HOCl for each laser pulse. The optical density of the HOCl sample was 1.0 OD/1.8 mm at the pump wavelength corresponding to a concentration of 0.17 M. Absorption spectra obtained before and after experiments were identical, demonstrating that no significant sample degradation occurred during the course of the experiment.

The details of the ultrafast transient absorption spectrometer have been presented elsewhere;[16] therefore, only a brief description is given here. A regenerative amplified titanium:sapphire laser producing 90-fs, 750-μJ pulses centered at 800 nm with a repetition rate of 1 kHz was employed in this work. The pump and probe pulses were produced as follows: The tunable pump pulses at 290, 310, and 330 nm were obtained by quadrupling the output from a traveling wave parametric generator (TOPAS) pumped by 480 μJ at 800 nm. The 266-nm pump pulse was generated by frequency tripling the 800-nm pulse whereas the 250-nm pulse was achieved by sum-frequency mixing the 800-nm pulse with the signal pulse from the TOPAS followed by frequency doubling. We obtained pulse energies on the order of 5−10 μJ that were tunable from 250 to 340 nm. The probe pulse was generated at 340 nm using a supercontinuum generated by focusing residual 800-nm light into a 2-mm ethylene glycol jet and subsequently frequency doubling a portion of the supercontinuum selected around 680 nm in a 1-mm BBO crystal. Because of dispersion in the optical setup and in the 1.8-mm flow cell, the temporal resolution is limited to ~700 fs in this work.

III. Results

The absorption spectrum of HOCl is composed of two absorption bands with maxima at 235 and 310 nm, respectively. The maximum at 310 nm is due to the $1^1A'' \leftarrow X^1A''$ electronic transition whereas the maximum at 235 nm is caused by the $2^1A' \leftarrow X^1A''$ electronic transition.[17,18] The two electronic transitions are only slightly blue-shifted ($\Delta\lambda \approx 5$ nm) compared

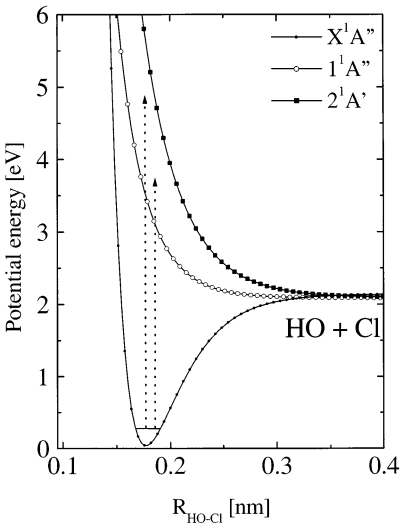

Figure 1. Gas-phase potential energy curves along the HO−Cl bond in HOCl from ref 17. The arrows represent different photolysis energies.

to the gas-phase values, indicating a modest solvent perturbation of the potential energy surfaces in the Franck−Condon region. Gas-phase photolysis studies of HOCl coupled with ab initio theoretical studies have given a detailed account of the yield of the photoproducts and the distribution of the excess energy among the translational and vibrational degrees of freedom.[19] The principal photodissociation products in the wavelength range from 140 to 440 nm are

$$\mathrm{HOCl}(\hat{\mathrm{X}}^1\mathrm{A}') + h\nu \rightarrow \mathrm{OH}(^2\Pi) + \mathrm{Cl}(^2\mathrm{P}) \qquad (1)$$

We previously studied in detail the photolysis of HOCl with 266-nm pump pulses and probe pulses in the range from 250 to 340 nm and observed that OH and Cl were formed with a near-unity quantum yield.[1] Since our time resolution is limited to approximately 0.7 ps, we are unable to confirm the hypothesis of a unity quantum yield directly. However, both a detailed analysis of the pump−probe excitation geometry[1] and a normalization of the data at 1 ps yield a near-unity quantum yield for dissociation, suggesting the absence of fast (<1ps) direct cage back-recombination Since the OH radical absorbs below 300 nm and the extinction coefficient of HOCl is very small (<100 L cm^{-1}/mol) relative to that of Cl, the transient absorption spectrum above 300 nm is solely due to the chlorine atoms formed in the photolysis of HOCl.[20,21] From the transient absorption spectrum, we can thus directly obtain the time dependence of the Cl concentration by selecting a probe wavelength above 300 nm where only the Cl fragments absorb. In this work, we have kept the probe wavelength constant at 340 nm and have scanned the photolysis wavelength across the absorption band of HOCl from 250 to 330 nm to monitor the dynamics of the photolysis as function of energy. In Figure 2, we show the time-dependent chlorine concentration for the five photolysis wavelengths employed in this work. As discussed in detail in ref 1, the dynamics of the chlorine concentration is caused by slow diffusive geminate recombination with OH radicals. For all of the pump wavelengths, the Cl concentration undergoes a nonexponential decay. At long delays (175 ps), the Cl concentration corresponds to ~35−60% of the initial value, depending on the wavelength. This level directly measures the fraction of Cl atoms that survives secondary geminate recombination, although a more precise determination of the long-time escape would require longer delays.[22] The experimental data at long delays obtained at a 266-nm pump

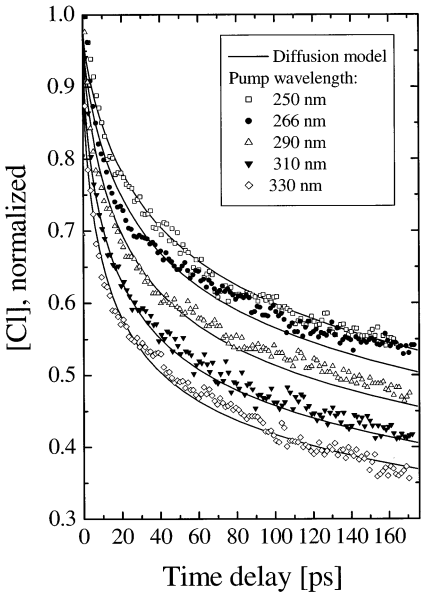

Figure 2. Time-dependent chlorine concentration shown for the different photolysis energies. The legend lists the photolysis wavelength and the derived excess kinetic energy. The partition between escape and recombination is approximately given by the concentration at 150 ps delay.

wavelength differs slightly from the other data sets, but given the low signal levels ($\Delta A < 10$ m OD) and the fact the 266-nm pump pulse was obtained using third-harmonic generation of the fundamental 800-nm pulse, we refrain from analyzing this deviation in greater detail. For high excitation energy, the kinetic energy imparted to the OH and Cl photofragments is high, leading to a large initial separation of the fragments and a low recombination yield. For low excitation energy, less energy is given to the fragments that, consequently, have a shorter initial separation, leading to a higher recombination yield.

IV. Analysis and Discussion

The large amount of excess energy available to the fragments following the photolysis of HOCl results in a large initial separation of the fragments and consequently a slow geminate recombination, as the photofragments must await diffusional encounters. The recombination dynamics reflected by the time-dependent Cl concentration therefore allows us to follow the solvent−solute interactions responsible for the thermalization of the hot fragments and the subsequent diffusion dynamics. In particular, the initial fragment separation $\langle r_0 \rangle$ and its dependence on the excess energy may be extracted from the Cl transient absorption using a model for the diffusive recombination. Thus, determining the initial fragment separation $\langle r_0 \rangle$ as a function of excess energy provides a measure of the solvent's stopping power.

Continuum Model: Spherical Symmetric Diffusion. Quantitatively, we model the slow recombination dynamics using numerical simulations of the spherical symmetric diffusion problem (SSDP). A simple and versatile software package, developed by N. Agmon and E. B. Krissinel, is available for solving the SSPD for a wide range of reaction types and boundary conditions.[14] Four parameters are needed in the simplest case to describe the dynamics of diffusive recombination between the Cl and OH radicals: (1) the relative diffusion coefficient of the Cl−OH fragments, $D_{Cl-OH} = D_{Cl} + D_{OH}$, (2) the reaction radius R_c where the recombination takes place, (3) the interaction potential $V(r)$ between the OH and Cl fragments in liquid water, and finally (4) the initial separation of the fragments at $t = 0$, $\langle r_0 \rangle$. The diffusion coefficient of OH in water is well known experimentally and is equal to 2.0×10^{-3} nm^2/ps.[23] In contrast, the diffusion coefficient of Cl(aq) has, to our knowledge, not been measured. However, using the self-diffusion coefficient of water and the estimated radius for Cl(aq), the diffusion coefficient has been estimated by Parson et al.:[24] $D_{Cl} \approx 1.0 \times 10^{-3}$ nm^2/ps. The relative diffusion constant thus becomes $D_{Cl-OH} = 3.0 \times 10^{-3}$ nm^2/ps. To estimate the reaction radius, we use the potential energy surface for the X^1A'' ground state of HOCl obtained from the ab initio calculations by Peterson et al.[18] We define the reaction radius as the internuclear distance (R_{Cl-OH}) where the potential energy is approximately equal to kT. For HOCl in the electronic ground state, the reaction radius is estimated to be $R_c \approx 0.35$ nm. When the Cl and OH fragments are separated by a distance equal to or less than R_c, they are assumed to recombine with unity yield, corresponding to the absorption boundary condition in the diffusion problem. The X^1A'' potential is well approximated by a 1D Morse potential along the R_{Cl-OH} coordinate,[25] and we use this as the interfragment potential energy in the simulation. This is similar to a recent simulation published by Bradforth on recombination in aqueous I^-.[26] As will be shown later, the choice of the intermolecular potential has only a weak influence on the parameters obtained, which is why we have chosen a simpler gas-phase potential instead of a mean-force potential that better takes into account the dynamic structure of the liquid solvent. Because of the high concentration of HOCl employed in this work, there is a small probability for secondary reactions between Cl and HOCl that could account for the additional loss of Cl atoms and the weak excess absorption due to the OH radical previously observed.[1] We have added a small sink term describing the slow loss of Cl atoms due to secondary reactions between Cl and HOCl. We describe the reaction as a pseudo-first-order reaction because of the high HOCl concentration and obtain a rate constant on the order 5×10^8 s^{-1}. The only remaining parameter in the SSDP model is thus the desired initial separation, which may be extracted by comparing the model with the experimental data shown in Figure 2. Because of the statistical nature of the thermalization process, a distribution of distances is expected rather than just a single value, and we therefore use a Gaussian distribution function defined by the peak position of the initial separation $\langle r_0 \rangle$ and the width σ of the distribution.

TABLE 1: Thermalization Distance $\langle r_0 \rangle$ (nm) as a Function of the Excess Energy ΔE[a]

wavelength (nm)	ΔE (eV)	$\langle r_0 \rangle_D$ (nm) $V = 0$	$\langle r_0 \rangle_D$ (nm) $V =$ Morse	$\langle r_0 \rangle_{MD}$ (nm) MD simulation
330	1.61	0.44	0.49	0.49
310	1.85	0.49	0.52	
290	2.13	0.53	0.57	0.51
266	2.52	0.58	0.60	
250	2.81	0.60	0.65	0.53

[a] $\langle r_0 \rangle_D$ denotes the peak of a Gaussian distribution function ($\sigma = 0.2$ nm) derived from the spherically symmetric diffusion model used to analyze the experimental data. The values of $\langle r_0 \rangle_D$ are listed both for the case where the interfragment interaction is governed by a Morse potential and for the case where the interaction is assumed to be zero. $\langle r_0 \rangle_{MD}$ denotes the separation obtained from an MD simulation of the fragment dynamics.

The simulated decay of the chlorine concentration obtained from the diffusion model is shown in Figure 2 together with the experimental data, and the parameters $\langle r_0 \rangle$ and σ are collected in Table 1. We obtain good agreement between experiment and simulation with the selected parameters, but it is possible to

obtain almost as good an agreement using a model with the interfragment potential set to zero. This gives a slightly smaller value of the initial fragment separation but the same dependence on the excess energy. The gas-phase value of the dissociation energy along the O−Cl coordinate is measured to be $D_0 = 2.39$ eV.[27,28] By taking into account the solvent from the estimated solvation energies for HOCl (0.3 eV),[29] OH (0.44 eV),[23] and Cl (0.1 eV),[30] we estimate a dissociation energy of 2.15 eV along the O−Cl coordinate of HOCl in aqueous solution. Subtracting 2.15 eV from the photon energy of the photolysis pulse gives the kinetic energy to be distributed among the OH and Cl photofragments.[31] We assume, on the basis of experimental evidence in the gas phase, that no excitation energy is used to excite the OH fragment vibrationally. In HOCl, the OH bond distance is very close to the O−H bond length found in the free hydroxyl radical and merely serves as a spectator mode remaining in the vibrational ground state.[2−4] The fragments rapidly lose this excess energy as a result of solvent−solute interactions. When the kinetic energy is on the order of kT, the fragments have thermalized, and thermal diffusion will determine their motion in the solvent. The diffusion model assumes that the fragments are in equilibrium with the surrounding solvent, and the good agreement with experimental data after 1 ps therefore suggests that $\langle r_0 \rangle$ of the diffusion model may be interpreted as the thermalization distance. The experimental data shown in Figure 2 therefore represents the ability of the solvent (H_2O) to thermalize the high-energy fragments. The experiments described here are thus similar to the classical stopping power measurements where the ability of solids and liquids to thermalize MeV particles were investigated.[32,33] The values of $\langle r_0 \rangle$ can be compared with the radius of the first and second solvation shells in pure liquid water.[34,35] These are approximately located at 0.28 and 0.5 nm, indicating that only two water molecules separate the fully thermalized fragments. This clearly demonstrates the efficiency by which the solvent, in the present case, water, is able to act as a sink for the excess energy released after the photodissociation. However, the short thermalization distances observed also suggest that a continuum description of the dissociation and recombination dynamics is likely to be an oversimplification.

Discrete Model: MD Simulation. To investigate the validity of the continuum approach and to assess the value of the parameters obtained, we performed a classical MD simulation of the HOCl(aq) system. The dissociation of electronically excited aqueous HOCl was investigated by applying classical molecular dynamics simulations to a system of 511 water molecules and 1 HOCl molecule. The weak absorption band of HOCl, peaking at 240 nm with a pronounced shoulder 300 nm, is caused by transition from the X^1A'' ground state to the purely repulsive $1^1A''$ and $2^1A'$ states. For the photolysis wavelengths used in this work, the exact contributions of the $1^1A''$ and $2^1A'$ states are unknown. Since the upper repulsive states are quite similar, we used the $1^1A''$ state to describe the dynamics of the dissociating HOCl molecule. The $^1A''$ state is known from the ab initio calculations of Nanbu and Iwata.[17] The initial geometry of the photolyzed molecule is assumed to be that of the ground-state equilibrium geometry, and the O−H bond length is kept fixed in agreement with the assumption that no vibrational excitation is expected in OH fragments. Additionally, we also choose to neglect the orientation of the OH fragment, defined through the angle θ between the OH bond and the relative velocity vector of the OH and Cl fragments. We use the potential energy of the repulsive state corresponding to the ground-state value of the HO−Cl angle equal to 102.45°. Because the simulation is primarily concerned with the separation of the fragments in the liquid solvent, this approximation is justified as the HOCl potential energy surface exhibited a strong θ dependence at the internuclear distances probed. If, however, we had included recombination in the model (i.e., included the ground-state potential surface and the nonadiabatic transition to the ground state), then the θ dependence would have been very important. Neglecting both vibrational and rotational excitation in the OH fragment means that all the excess energy is deposited into the kinetic energy of the fragments. On the basis of the dissociation and hydration energies discussed in the previous section, we subtract 2.15 eV from the photon energy of the photolysis pulse to obtain the kinetic energy to be distributed among the OH and Cl photofragments.

The water−water interaction was described by adopting the SPC-flexible model.[36] To model the electrostatic interactions between one HOCl and one H_2O molecule, a simple restricted Hartree−Fock calculation,[37] carried out at the experimental equilibrium geometry of HOCl, was used to assign Mulliken point charges to the atoms of HOCl. In the calculation, we used the cc-pVDZ basis set. The charges on H, O, and Cl were found to $0.40e$, $-0.43e$, and $0.03e$, respectively. In the simulation, we adopted the charges $0.43e$, $-0.43e$, and $0e$, respectively. To model the dispersion interaction between Cl in HOCl and the atoms in H_2O, Lennard-Jones parameters for H−Cl and O−Cl interactions were found by applying standard Lorentz−Berthelot mixing rules.[38] A molecular dynamics simulation with a fixed number of molecules and a fixed volume and energy (NVE) employing 511 SPC water molecules and 1 HOCl molecule was performed using a box length of 24.89 Å corresponding to a density of 0.997 g/cm^3. A half-box-length spherical cutoff together with standard periodic boundary conditions was applied. The average temperature was set to 298 K through an equilibration run. In this run, the geometry of the HOCl molecule was kept fixed at the calculated geometry of Nanbu and co-workers[17] by adopting the SHAKE routine by Ryckaert et al.[39] After equilibration, the program was run for 130 ps using a time step of 1 fs. For every 2.5 ps, the positions and momenta of all the molecules were stored for later use in the analysis of the dissociation dynamics of HOCl. During dissociation, the value of the R_{O-Cl} coordinate was recorded for every 0.125 fs. In none of the trajectories did the separation between the fragments exceed the half box length, and only a slight temperature increase of less than 5° was observed. Because we are far from a phase transition, we do not expect that such a small temperature increase will influence our results. A total of 51 trajectories were carried out for each of the pump wavelengths: 330, 290, and 250 nm, chosen to match the experimental pump wavelengths.

In Figure 3, we show the time-dependent fragment velocity and distance (R_{HO-Cl}) as a function of time. During the first 20 fs after photodissociation, the fragments separate ballistically to a distance of 0.3 nm before interaction with the solvent slows down the fragments, resulting in an outer turning point at $R_{HO-Cl} \approx 0.53-0.60$ nm depending on the photolysis wavelength. The impact of the dissociating fragments leads to a compression of the surrounding solvent, which forces the fragments back to a thermalization distance of ~0.49 to 0.53 nm, measured after 0.5 ps. The thermalization distances derived from experiments and MD simulation are compared in Figure 4. The magnitudes of the thermalization distances obtained are in reasonable agreement, both resulting in a thermalization distance corresponding to two to three water molecules. Moreover, both models yield an increasing fragment separation with photolysis

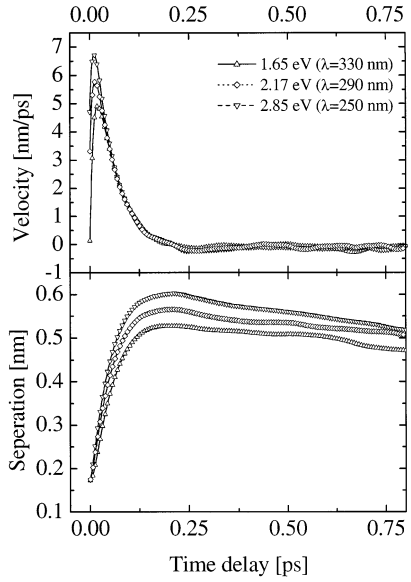

Figure 3. Results from the MD simulation giving the separation of the fragments and the relative velocity. The thermal velocity is given as the dotted line. The first 20 fs is the ballistic phase after which the influence of the solvent appears. After roughly150 fs, the fragments reach thermal velocities.

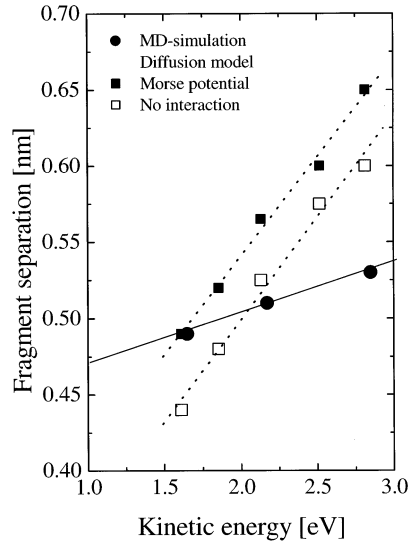

Figure 4. Excess energy dependence of the initial separation of the fragments, $\langle r_0 \rangle_D$ obtained from the experimental data when analyzed by the spherically symmetric diffusion model and the initial separation obtained from the MD simulations.

energy, but the slope resulting from the MD simulations is a factor of 3.3 smaller than that extracted from the experiment. Thus, the thermalization distances obtained from experiment may be fitted to a straight line with a slope of 0.13 nm/eV whereas the MD simulation gives a straight line with a significantly smaller slope of 0.04 nm/eV.

The thermalization of the photofragment kinetic energy is caused by the interaction between the solvent and the solute and can qualitatively be linked to the presence and strength of the intermolecular forces of the solvent. The process of kinetic energy relaxation is related to the process of vibrational relaxation since the solvent degrees of freedom are similar.[40] Our experimental data seem to suggest that the solvent, liquid water, is less capable of dissipating the fragment kinetic energy as compared to the discrete model based on the properties of pure (SPC) water. In other words, SPC water seems to overestimate the stopping power of liquid water. For the chlorine fragment, the interaction with the solvent is quite weak and thus relatively insensitive to the detailed nature of the MD simulation. For the OH fragment, however, we expect a strong interaction with the solvent, in particular through hydrogen bonding. The SPC model gives a poor representation of the hydrogen bond network[41] and is therefore expected to underestimate the solvent's ability to thermalize the energetic hydroxyl radicals, in contrast to the observed overestimation. However, the validity of such arguments is based on the assumption of weak coupling between the solvent and solute degrees of freedom. Given the large value of the kinetic energy, $E_{kin} \approx$ 2.5 eV, the short thermalization distances, and the correspondingly short thermalization time, the weak-coupling assumption is highly questionable, and a more elaborate theoretical treatment of the problem is desirable. Alternatively, one could view the process as a caging of the fragments between the first and second solvation shells. The thermalization distances obtained are approximately located at the second solvation shell. In this picture, the (weak) increase in thermalization distance with photolysis energy could be interpreted as a temporary expansion of the solvent shell caused by the impact of the energetic fragments. There is some support for this picture in the MD simulations shown in Figure 3, where the fragment separation actually decreases slightly following the maximum at 200 fs as a result of the elastic properties of the solvent shell. However, the time scale for relaxation of this perturbation of the second solvent shell is expected to be very fast, less than 1 ps, according to the MD simulation. It is therefore unlikely to contribute to the long-time recombination dynamics and in particular to the observed energy dependence. Again, a more elaborate theoretical treatment would be desirable; in particular, an MD simulation utilizing a much larger box size and longer times would be of interest to determine if the equilibrium diffusive properties of the OH and Cl fragments would appear before recombination, as the apparent success of the continuum model seems to indicate.

In conclusion, we have performed an experimental study of the photolysis of aqueous HOCl. From an earlier study, it is known that HOCl dissociates with a near-unity quantum yield into OH and Cl, which subsequently recombine geminately in a diffusion-limited process. Using femtosecond transient absorption spectroscopy, we have followed the changes in the dynamics of the geminate recombination as the photolysis wavelength was gradually blue shifted, thereby imposing more kinetic energy to the photofragments, enabling them to separate more before they thermalize and recombine. The kinetic energy of the fragments ranges from approximately 1.5 to 3 eV, and the fragments are observed to have thermalized when they are separated by $\langle r_0 \rangle = 0.4$ to 0.7 nm, corresponding to two to three water molecules. $\langle r_0 \rangle$ increases with fragment energy with a slope of approximately 0.13 nm/eV. In a simple MD simulation, we have obtained qualitative agreement with the experimental data, although the calculated stopping power of the solvent appears more effective compared to that inferred from the experimental data.

References and Notes

(1) Thomsen, C. L.; Madsen, D.; Poulsen, J. A.; Thogersen, J.; Jensen, S. J. K.; Keiding, S. R. *J. Chem. Phys.* **2001**, *115*, 9361−9369.

(2) Hickman, C. G.; Brickell, A.; Frey, J. G. *Chem. Phys. Lett.* **1991**, *185*, 101−104.

(3) Hickman, C. G.; Shaw, N.; Crawford, M. J.; Bell, A. J.; Frey, J. G. *J. Chem. Soc., Faraday Trans.* **1993**, *89*, 1623−1630.

(4) Bell, A. J.; Pardon, P. R.; Hickman, C. G.; Frey, J. G. *J. Chem. Soc. Faraday Trans.* **1990**, *86*, 3831−3836.

(5) Apkarian, V. A.; Schwentner, N. *Chem. Rev.* **1999**, *99*, 1481−1513.
(6) Vorsa, V.; Nandi, S.; Campagnola, P. J.; Larssin, M.; Lineberger, W. C. *J. Chem. Phys.* **1996**, *106*, 1402−1410.
(7) Wan, C.; Gupta, M.; Baskin, J. S.; Kim, Z. H.; Zewail, A. H. *J. Chem. Phys.* **1997**, *106*, 4353−4356.
(8) Thogersen, J.; Thomsen, C. L.; Poulsen, J. A.; Keiding, S. R. *J. Phys. Chem. A* **1998**, *102*, 4186−4191.
(9) Shin, K. J.; Kapral, R. *J. Chem. Phys.* **1978**, *69*, 3685−3696.
(10) Sano, H.; Tachiya, M. *J. Chem. Phys.* **1979**, *71*, 1276−1282.
(11) Smoluchowski, M. V. *Z. Phys. Chem., Stoechiom. Verwandtschaftsl.* **1917**, *92*, 129.
(12) Noyes, R. M. *J. Chem. Phys.* **1954**, *22*, 1349.
(13) Otto, B.; Schroeder, J.; Troe, J. *J. Chem. Phys.* **1984**, *81*, 202−213.
(14) Krissinel, E. B.; Agmon, N. *J. Comput. Chem.* **1996**, *17*, 1085−1098.
(15) Cady, G. H. *Inorg. Synth.* **1955**, *5*, 156.
(16) Thomsen, C. L.; Madsen, D.; Thogersen, J.; Byberg, J. R.; Keiding, S. R. *J. Chem. Phys.* **1999**, *111*, 703−710.
(17) Nanbu, S.; Iwata, S. *J. Phys. Chem.* **1992**, *96*, 2103−2111.
(18) Peterson, K. A.; Skokov, S.; Bowman, J. M. *J. Chem. Phys.* **1999**, *111*, 7446−7456.
(19) Offer, A. R.; BalintKurti, G. G. *J. Chem. Phys.* **1995**, *104*, 563−575.
(20) Klæning, U. K.; Wolff, T. *Ber. Bunsen-Ges. Phys. Chem. Chem. Phys.* **1985**, *89*, 243.
(21) Pagsberg, H.; Christensen, H.; Rabini, J.; Nielsson, G.; Fenger, J.; Nielsen, S. O. *J. Phys. Chem.* **1969**, *73*, 1029.
(22) Crowell, R. A.; Bartels, D. M. *J. Phys. Chem.* **1996**, *100*, 17940−17949.
(23) Buxton, G. V.; Greenstrock, C. L.; Hellman, W. P.; Ross, A. B. *J. Phys. Chem. Ref. Data* **1988**, *17*, 513−531.
(24) Parsons, R. *Handbook of Electrochemical Constants;* Butterworths Scientific Publications: London, 1959.
(25) $V(R) = 82(1 - \exp(3(r - 1.77))^{**}2$.
(26) Kloepfer, J. A.; Vilchiz, V. H.; Lenchenkov, V. A.; Chen, X.; Bradforth, S. E. *J. Chem. Phys.* 2002, in press.
(27) Barnes, R. J.; Dutton, G.; Sinha, A. *J. Phys. Chem.* **1997**, *101*, 8374−8377.
(28) Wedlock, M. R.; Jost, R.; Rizzo, T. R. *J. Chem. Phys.* **1997**, *107*, 10344−10347.
(29) Geiger, F. M.; Hicks, J. M.; Dios, A. C. d. *J. Phys. Chem.* **1998**, *102*, 1514−1522.
(30) Sevilla, M. D.; Summerfield, S.; Eliezer, I.; Rak, J.; Symons, M. C. R. *J. Phys. Chem.* **1997**, *101*, 2910−2915.
(31) We assume that no vibrational excitation of OH is present.
(32) Lindhard, J.; Scharff, M. *Kgl. Danske Videnskabers Selskab. Mat-Fys. Medd.* **1953**, *27*.
(33) Bethe, H. A.; Ashkin, J. Passage of Radiation Through Matter. In *Experimental Nuclear Physics;* Segre, E., Ed.; Wiley: New York, 1953; Vol. 1, pp 166−201.
(34) Agmon, N. *J. Chem. Phys.* **1996**, *100*, 1072−1080.
(35) Narten, A. H.; Levy, H. A. *J. Chem. Phys.* **1971**, *55*, 2263.
(36) Toukan, K.; Rahman, A. *Phys. Rev. B* **1985**, *31*, 2643−2648.
(37) Frisch, M. J.; Trucks, G. W.; Schlegel, H. B.; Scuseria, G. E.; Robb, M. A.; Cheeseman, J. R.; Zakrzewski, V. G.; Montgomery, J. A., Jr.; Stratmann, R. E.; Burant, J. C.; Dapprich, S.; Millam, J. M.; Daniels, A. D.; Kudin, K. N.; Strain, M. C.; Farkas, O.; Tomasi, J.; Barone, V.; Cossi, M.; Cammi, R.; Mennucci, B.; Pomelli, C.; Adamo, C.; Clifford, S.; Ochterski, J.; Petersson, G. A.; Ayala, P. Y.; Cui, Q.; Morokuma, K.; Malick, D. K.; Rabuck, A. D.; Raghavachari, K.; Foresman, J. B.; Cioslowski, J.; Ortiz, J. V.; Stefanov, B. B.; Liu, G.; Liashenko, A.; Piskorz, P.; Komaromi, I.; Gomperts, R.; Martin, R. L.; Fox, D. J.; Keith, T.; Al-Laham, M. A.; Peng, C. Y.; Nanayakkara, A.; Gonzalez, C.; Challacombe, M.; Gill, P. M. W.; Johnson, B. G.; Chen, W.; Wong, M. W.; Andres, J. L.; Head-Gordon, M.; Replogle, E. S.; Pople, J. A. *Gaussian 98*; Gaussian, Inc.: Pittsburgh, PA, 1998.
(38) Allan, M. P.; Tildersly, D. J. *Computer Simulations of Liquids;* Oxford University Press: Oxford, U.K., 1987.
(39) Ryckaert, J. P.; Ciccotti, G.; Berendsen, H. J. C. *J. Comput. Phys.* **1977**, *34*, 327.
(40) Owrutsky, J. C.; Raftery, D.; Hochstrasser, R. M. *Annu. Rev. Phys.Chem.* **1994**, *45*, 519−555.
(41) Heyes, D. M. *J. Chem. Soc., Faraday Trans.* **1994**, *90*, 3039−3049.